Accepted in Experimental Mechanics

The Combined Effects of Moisture and Temperature on the Mechanical Response of Paper

Eric Linvill · Sören Östlund

Abstract To model advanced 3-D forming strategies for paper materials, the effects of environmental conditions on the mechanical behavior must be quantitatively and qualitatively understood. A tensile test method has been created, verified, and implemented to test paper at various moisture content and temperature levels. Testing results for one type of paper for moisture contents from 6.9 to 13.8 percent and temperatures from 23 to 168 degrees Celsius are presented and discussed. Coupled moisture and temperature effects have been discovered for maximum stress. Uncoupled effects have been discovered for elastic modulus, tangent modulus, hardening modulus, strain at break, tensile energy absorption (TEA), and approximate plastic strain. A hyperbolic tangent function is also utilized which captures the entire one-dimensional stress-strain response of paper. The effects of moisture and temperature on the three coefficients in the hyperbolic tangent function may be assumed to be uncoupled, which may simplify the development of moisture- and temperature-dependent constitutive models. All parameters were affected by both moisture and temperature with the exception of TEA, which was found to only be significantly dependent on temperature.

E. Linvill
KTH Royal Institute of Technology
Department of Solid Mechanics
SE - 100 44 Stockholm
Tel.: +46-76-5946093
E-mail: linvill@kth.se

S. Östlund
KTH Royal Institute of Technology
Department of Solid Mechanics
SE - 100 44 Stockholm
Tel.: +46-8-7907542
E-mail: soren@kth.se

Keywords Moisture · Temperature · Elastic Properties · Plastic Properties · Forming · Paper

Background

Although it is one of the oldest human-made materials, paper continues to develop as an increasingly versatile engineering material. Modern paper packages are required to perform equally well in highly varied environments without failure. Effort is additionally being placed into reducing the amount of raw material in each package to lessen shipping weight and environmental impact. Furthermore, more complex, 3-D forming strategies are being developed [1, 2, 3, 4] to create greater diversity and possibilities among paper packaging. A 3-D forming process is defined in this paper as any process which converts paperboard into a 3-D packaging structure. Advanced 3-D forming processes typically need to utilize moisture and/or temperature application for 3-D forming success.

Finite element simulation can be extremely helpful in the development of manufacturing strategies. However, good constitutive models are required to produce meaningful simulations of 3-D forming. Effort has recently been placed into developing good constitutive models for paper materials [5, 6, 7], but none of these models take into consideration the combined effects of moisture and temperature on the mechanical response of paper. Before attempting to model the effects of moisture and temperature on the 3-D deformation properties of paper, the tensile, one-dimensional properties must first be better understood. The tensile response is of greatest interest, because compressive stresses during 3-D forming will typically cause elastic instability (i.e. buckling). Previous experimental studies have been conducted to explore the independent effects of moisture and temperature on the elastic properties of paper, but very little experimental work has considered effects of moisture and temperature on the plastic (permanent deformation) properties of paper or the combined effects of moisture and temperature on the entire, one-dimensional, tensile, mechanical response of paper.

Effects of Moisture

Moisture is widely known to have a significant impact on the constitutive behavior of paper materials [8, 9, 10, 11, 12, 13]. The moisture content of paper will be defined with the following relationship:

$$mc = \frac{M_{moist}}{M_{tot}} = \frac{M_{tot} - M_{dry}}{M_{tot}} \tag{1}$$

where mc is the moisture content, M_{moist} is the mass of moisture contained within the paper, M_{tot} is the total mass of the paper including the moisture, and M_{dry} is the mass of the paper when dry.

The effect of moisture on the elastic modulus of paper is probably the best understood and most comprehensively modeled of all effects on paper's constitutive behavior. The softening effect of water on paper has been modeled by Nissan's hydrogen-bond dissociation theory [14]. This theory predicts a change of the elastic modulus in the following form for moisture content levels above five percent:

$$ln\left(\frac{E}{E_0}\right) = A - B \cdot mc \tag{2}$$

where E is the elastic modulus, E_0 is the elastic modulus at zero percent moisture content, and A and B are constants. The constant B in Nissan's equation is similar (almost equal) for all types of paper, which allows one to calculate the elastic modulus of the paper at any moisture content greater than five percent given the elastic modulus at any moisture content greater than five percent.

While the description of the softening effect of moisture is fairly well defined for the elastic response, there has been very little research into the effect of moisture on the plastic or entire mechanical response of paper materials. One attempt to experimentally determine the effect of moisture content on plastic strain was by Land et al. [9]. Utilizing standard testing procedures proved too difficult to determine the plastic strain during each test, so Land et al. utilized cyclic loading and unloading increments to determine the amount of accumulated plastic strain on each load cycle. While this testing method proved to be more

successful in determining the plastic strain than utilizing standard tests, no model could be created from the results to describe how the relationship between stress and plastic strain is affected by moisture (although the results imply that the moisture content has some effect on the plastic response).

One attempt to describe the effect of moisture on the entire mechanical response is given by Yeh et al. [10]. Yeh et al. utilizes the hyperbolic tangent function to describe the mechanical response of paper, and this function fits very well to paper's one-dimensional mechanical response. This hyperbolic tangent function is different from the hyperbolic function utilized by Gunderson et al. [13] and Erkkilä et al. [15] which has one less constant but poorer fitting accuracy than the hyperbolic tangent function utilized by Yeh et al. [10]. Yeh et al. states that the coefficients of their hyperbolic tangent function are linearly dependent on the moisture content. Similarly, Benson [16] found a linear relationship between moisture content and both maximum stress and modulus of elasticity.

Moisture is known to be absorbed into the paper structure in two ways: water molecules can bind with OH groups (i.e. bound water), or liquid water can fill the larger pores of the paper structure through capillary condensation (i.e. unbound water) [17]. Additionally, the bound water can be in either a freezing or non-freezing form, although the freezing form typically does not occur in cellulose at moisture contents less that 20 % [18, 19]. The theory developed by Nissan [14] assumes that the effect of unbound water on the mechanical response is negligible and that the hydrogen bonding (i.e. non-freezing bound water) has the greatest impact on mechanical properties. Moisture contents throughout this work do not exceed 14 %, so the effects of moisture seen in this work are most likely due to differing amounts of non-freezing bound water.

Effects of Temperature

Similar to moisture, temperature is also known to have a significant impact on the constitutive behavior of paper [20, 11]. A similar form of Nissan's hydrogen bond theory can be utilized to describe the change in elastic modulus dependent on the change in temperature [11]. This relationship is given by:

$$\frac{dln(E)}{dT} = K \tag{3}$$

where E is the elastic modulus, T is the temperature, and K is a constant. The estimated value of the constant K for paper by Nissan's theory is 0.0031 $^{\circ}C^{-1}$ [21].

Salmén and Back [21] conducted extensive testing to explore the effect of temperature on the elastic modulus and ultimate strength of dry paper. Their testing found that paper experiences a relationship between elastic modulus and temperature as described by Nissan's theory. The constant K as described by the testing was found to be in the range of 0.0025 to 0.0037 $^{\circ}C^{-1}$, which supports the relationship from Nissan's hydrogen bond theory.

Contrary to Nissan's hydrogen bond theory, Benson [16] discovered linear relationships between temperature and three mechanical response parameters: elastic modulus, strain at break, and maximum stress.

Similar to moisture, the existing theories are only successful in describing the effect of temperature on the elastic response of paper. No studies have attempted to explore the effect of temperature on the entire, one-dimensional, tensile, mechanical response of paper.

Combined Effects of Temperature and Moisture

Salmén and Back [22] were able to experimentally show that the medium in which one tests paper (whether or not it can absorb moisture) has negligible effect on the mechanical response. This result implies that the transport of moisture into the environment is negligible during the time range that is typical for tensile testing of paper for the range of environments used by Salmén and Back [22].

The effects of moisture content and temperature on the mechanical response of paper are not necessarily independent from each other. The study by Benson [16] noted that the effect of temperature on paper's mechanical response is dependent on the ambient relative humidity. However, no experimental studies have explored how the effects of moisture and temperature are coupled. Further testing is therefore required to explore the coupled effects of moisture and temperature on the mechanical response of paper.

Experimental Setup and Method

All tensile test specimens were produced from hand sheets utilizing a Celeste kraft pulp from SCA (Svenska Cellulosa Aktiebolaget). Beating curves were generated for hand-sheets created from the base pulp. A beating value of 160 KWh/t in conjunction with white water recirculation, which provides the best strain-at-break properties for hand-sheets made from this base pulp, was chosen. Strain at break was selected as the driving parameter, because this study has a 3-D forming focus; greater strain at break is most likely better for the 3-D forming of complex shapes. The hand-sheets were formed utilizing a Rapid Köthen laboratory sheet former available in the Department of Fibre and Polymer Technology at KTH Royal Institute of Technology. Hand sheets as opposed to machine made paper were utilized for the experiments with the intention that future experimentation on chemically and/or mechanically modified handsheets utilizing the same base pulp will be conducted. The mean structural thickness of each hand-sheet was found utilizing the SCAN-P88:01 test method. The mean thicknesses of specimens utilized for this study ranged from 190 to 200 μm.

All specimens were conditioned at the desired relative humidity and 23 degrees Celsius in the climate room at the Department of Solid Mechanics at KTH Royal Institute of Technology. One hand sheet was weighed on a balance in the dry state and weighed on a balance at each relative humidity setting in order to calculate the moisture content through *Equation (1)*. All specimens were conditioned at least 14 hours and were tested at the same relative humidity level that they were conditioned at.

The tensile testing utilized the Instron ElectroPuls E1000 test frame equipped with a 250-Newton load cell. The test setup is illustrated in *Figure 1*. Heat was applied to the top and bottom sides of the specimen utilizing two heat lamps, as shown in *Figure 1*. The output of the heat lamps was controlled using a power regulator, and the specimen was radiated by the heat lamps from a distance of approximately 4 cm. To determine the approximate temperature of the specimens during the experiment, a temperature probe was placed in the specimen's location, and the different power output settings were applied. The equilibrium temperature of the probe was chosen as the approximate temperature of the specimen during

the test. The temperature of the load cell was also measured at the greatest heat output setting, and this temperature never exceeded the operational temperature of the load cell.

Specimens were cut into 50 mm by 15 mm strips, and the actual test length was 35 mm. The specimens were chosen to be smaller than the standard tensile test size of a paper specimen for two reasons: the temperature application method and the limited raw material. Utilizing a longer test piece would provide unequal temperature distributions within the paper specimen due to the geometry of the heat lamps. Additionally, having specimens of this size significantly reduced the required number of manufactured hand sheets. Recent research by Hagman and Nygårds [23] has shown a dependency of tensile testing results on specimen size for paper. Since the length of the specimens in this study is less than the standard sample size, then, according to the results given by Hagman and Nygårds [23], higher values for strain at break and stiffness are expected compared to a standard test specimen size. However, since the same sample length is utilized throughout this study, the size effect should not significantly impact the results.

During the testing sequence, the specimen was first placed and fastened into the clamps, then the heat lamps were placed in position. The power was applied to the heat lamps, and immediately afterwards the start button was pressed. The tensile testing program utilized consistently had a four-second processing time (as measured by stopwatch) between when the start button was pressed and when the test actually started. This processing time allowed for the specimen to heat up from the radiation but not be so long as to dry out (verification of this statement is provided in the following section). The tests were all conducted at 0.25 mm/s, which corresponds to a strain rate of 0.7 %/s. This rate was chosen in order to reduce viscous stiffening effects while keeping the test short enough to prevent drying of the specimen while subject to high temperatures. The longest tensile test lasted eight seconds, which provides a maximum heat application time of 12 seconds. The outputs from the tensile tests were force from the load cell and displacement of the cross-head.

The temperature and moisture conditions chosen for the testing are displayed in *Table 1*. The boxes in *Table 1* marked with an X are the moisture-temperature combinations which were tested. At least five specimens were tested at each of these combinations.

Evaluating Moisture Change

In order to experimentally determine the moisture loss due to high temperature application, a 50-gram load cell was utilized in combination with a clamping system utilizing a steel wire and a paper-clip. The test setup is displayed in *Figure 2*. The clamping system in *Figure 2* kept the load cell out of the radiation path of the heat lamps. One specimen was conditioned at 90 percent relative humidity (RH) while another specimen was conditioned at 50 percent RH. The tested specimen was placed in the clamp, then the heating lamps were set to to the greatest power output utilized during the tensile tests, equivalent to 168 degrees Celsius. The result of the moisture loss verification test is shown in *Figure 3*. *Figure 3* illustrates the greatest amount of moisture loss at the lowest and highest RH settings utilized throughout the experiments. A trend line is utilized, because the sensitivity of the load cell provided some scatter in the results. This sensitivity was caused by the fact that the specimen weighed about half a gram while the load cell was designed to measure greater loads. *Figure 3* shows that a negligible amount of moisture is lost at low RH and high temperatures, while some moisture is lost at high RH and high temperature. Approximately four percent moisture content was lost at the most severe condition, which could have some impact on the final results for combinations of high RH and high temperature. A study of how the strain at break and maximum stress results would be affected by this moisture loss is presented in *Appendix A*.

The change in moisture content caused by the application of high temperature would be greatest for failure properties; the specimens could have been exposed to up to 12 seconds of high temperature at failure. On the contrary, little effect of drying is expected on initial properties, and small effect is expected on permanent deformation properties. However, the result for the specimen at 90 % RH in *Figure 3* only represents the scenario at which the moisture loss would be greatest. Additionally, the tests at high temperature were typically shorter than the maximum of 12 seconds, because increased temperature reduces the strain at break of paper. Therefore, the change in moisture content due to drying is expected to be negligible for the constitutive properties, while some skepticism is kept for the analysis of failure properties at high temperatures.

Mechanosorption, the change in moisture content caused by straining, is known to be prevalent in paper materials. This could cause the moisture content of a specimen to change throughout the test. However, results by Gunderson [24] have shown an increase of moisture content only as great as 0.05 % at 50 % RH and at 50 % of the strain at break. Although this value could be greater at greater relative humidities, the effect of mechanosorption on the tests is assumed to be negligible.

An analysis of other measurement errors and their maximum effects on the results is provided in *Appendix B*.

Results and Discussion

The results of the testing are split into two separate sections: constitutive properties and failure properties. The constitutive properties studied include the three constants in the hyperbolic tangent function utilized by Yeh et al. [10], elastic modulus, tangent modulus, and hardening modulus. The failure properties investigated include maximum stress, strain at break, tensile energy absorption (TEA) and approximate maximum plastic strain.

Each property investigated in this study is displayed in two separate graphs: one dependent on moisture and the other dependent on temperature. In the graphs with moisture on the independent axis, the mean for each data point (i.e. each moisture-temperature combination) is marked and single standard deviation bars are provided to illustrate the variability. Similarly, the graphs with temperature on the independent axis are marked at the mean for each data point and single standard deviation bars are provided. General isotherm (constant temperature) and isohume (constant relative humidity and thus moisture content) trend lines to help the reader more easily visualize the trends that occur in each graph.

The terms *coupled* and *uncoupled* are utilized extensively throughout this section. Material properties which are coupled experience effects of moisture and temperature which are dependent on each other. On the contrary, material properties which are uncoupled experience independent effects of moisture and temperature. Uncoupled material properties are typically easier to describe through constitutive relationships than coupled properties. Analysis of variance (ANOVA) and non-linear regression analysis have been chosen to determine

whether the effects of moisture and temperature on each material property are uncoupled or coupled. ANOVA or regression analyses produce a p-value for each constant; this p-value describes the importance of each constant (i.e., the smaller the p-value is, the more influence the constant has on the final model). Additionally, linear coupling can be graphically visualized; parallel isotherm or isohume trend lines indicate that uncoupled linear behavior likely exists.

Constitutive Properties

The hyperbolic tangent function was utilized to fit the tensile response of each specimen utilizing a Levenberg-Marquardt algorithm. The utilized hyperbolic tangent function is given by:

$$\sigma = C_1 \tanh(C_2 \varepsilon) + C_3 \varepsilon \tag{4}$$

where σ is the stress, C_1, C_2, and C_3 are fit coefficients, and ε is the strain. This function is useful, because it captures the transition from elastic to plastic deformation well. An example of the hyperbolic tangent function as described by *Equation (4)* is displayed in *Figure 4*. The hyperbolic tangent function captures well the tensile, one-dimensional mechanical response of paper materials; C_3 is typically set to zero for compressive, one-dimensional loading. *Figure 4* shows one of the experimental results and the ability of the hyperbolic tangent function to fit the experimental result very well. The R-squared values, which describe how well the experiments are matched by the hyperbolic tangent function in *Equation (4)*, were all greater than 0.999.

The p-values for the uncoupled and coupled effects of moisture and temperature on each constitutive parameter calculated through ANOVA are displayed in *Table 2*. Green numbers in *Table 2* indicate that the variable (temperature, moisture, or moisture and temperature) has an impact on the parameter with 95 % confidence, while brown numbers indicate that the variable has no impact on the parameter with 95 % confidence. Therefore, a brown number

in the *Temperature and Moisture* column shows that the effects of moisture and temperature on the material property are uncoupled.

The results for C_1 are shown in *Figure 5*. There is slight coupling of the effects of moisture and temperature on C_1, as shown in *Table 2*. However, the value of C_1 appears to be affected exponentially by both moisture content and temperature, as seen in *Figure 5*. While ANOVA calculates coupling based on linear relationships between independent variables (i.e. temperature, moisture, and temperature and moisture) and dependent variables (i.e. C_1), a non-linear regression analysis can be conducted utilizing an exponential relationship:

$$C_1 = \beta_1 e^{-\beta_2 \cdot mc - \beta_3 \cdot T - \beta_4 \cdot mc \cdot T} \tag{5}$$

where β_{1-4} are constants. The result of such a regression analysis gives p-values as shown in *Table 3*, where values above 0.05 (colored brown) are parameters which do not have an impact on C_1 with 95 % confidence. *Table 3* shows that the coupling term (i.e. β_4) can be ignored if the model for C_1 is given by *Equation (5)*. This result implies that an uncoupled, non-linear model can be utilized to describe the effects of moisture and temperature on C_1.

The results for C_2 are displayed in *Figure 6*. *Figure 6* shows uncoupled effects of moisture and temperature on C_2, as is supported by *Table 2*. The relationships between C_2 and both the moisture content and temperature are fairly linear with a few exceptions. The value of C_2 does not considerably change the overall shape of the hyperbolic tangent function (i.e. C_2 affects how sharp of the transition from purely elastic to plastic loading is), so the few exceptions should not be a significant issue from a modeling perspective.

The results for C_3 are displayed in *Figure 7*. An uncoupled response between the effects of moisture and temperature on the C_3 value is shown in *Figure 7* and is supported by *Table 2*. The trends appear to follow a linear behavior. Taking the derivative of *Equation (4)* with respect to strain gives:

$$\frac{d\sigma}{d\varepsilon} = C_1 C_2 \left(1 - \tanh^2 \left(C_2 \varepsilon\right)\right) + C_3 \tag{6}$$

where σ is the stress, ε is the total strain, and C_1, C_2, and C_3 are fit coefficients. *Equation (6)* shows that as the total strain approaches infinity, the slope of the stress-strain curve approaches C_3. Therefore, C_3 and the tangent modulus should be approximately equal in magnitude.

An interesting result from the analysis of the experiments utilizing the hyperbolic tangent function is that all three fit parameters could be assumed to be affected by moisture and temperature in an uncoupled manner. This phenomenon may be useful in developing constitutive relations which are dependent on moisture and temperature.

The elastic modulus was calculated by evaluating *Equation (6)* at zero strain:

$$E = C_1 C_2 + C_3 \tag{7}$$

The results of *Equation (7)* for the elastic modulus are displayed in *Figure 8*. Coupled effects of moisture and temperature on the elastic modulus are apparent in *Figure 8* and *Table 2*. The dependency of elastic modulus on moisture content shows a linear relationship, which matches the results seen by Benson [16] but not the trends as predicted by Nissan [14]. The effect of temperature on elastic modulus (whether the trends are linear, exponential, or another relationship) is not obvious. Utilizing the same non-linear regression approach as utilized to analyze C_1, the elastic modulus may be assumed to be:

$$E = \beta_1 e^{-\beta_2 \cdot mc - \beta_3 \cdot T - \beta_4 \cdot mc \cdot T} \tag{8}$$

where β_{1-4} are constants. The result of a regression analysis utilizing the model in *Equation (8)* are displayed in *Table 4*. The p-value for β_4 in *Table 4* is barely greater than 0.05, which means that the effect of coupling for the model described by *Equation (8)* can be ignored with almost exactly 95 % confidence. The exponential model given by *Equation (8)* supports the models utilized by Nissan [14], Salmén and Back [21], and Haslach [11].

The tangent modulus is the slope of the stress-strain curve in the plastic region and was calculated by finding the slope of the stress-strain curve from 1.0 % to 0.5 % strain before failure. The results for the tangent modulus are displayed in *Figure 9*. The uncoupled effects

of moisture and temperature on the tangent modulus seen in *Figure 9* are further supported by the results in *Table 2*. The trends also appear to be described very well by a linear fit with the exception of the questionable results at 114 ^{o} C and 11 % moisture content. This outlier is most likely caused by uncertainty in the results due to the limited number of specimens. The results are similar to those for C_3 shown in *Figure 7*, which is expected.

The hardening modulus was calculated utilizing a small strain approach by:

$$\frac{1}{H} = \frac{1}{E_{tan}} - \frac{1}{E} \tag{9}$$

where H is the hardening modulus and E_{tan} is the tangent modulus. Therefore, the hardening modulus is a measurement of the slope of the linear relationship between plastic strain and stress at large plastic strain values. The results for the hardening modulus are displayed in *Figure 10*. Similar to the results in *Figure 9*, although the trends are marginally less clear, *Figure 10* shows uncoupled, linear effects of moisture and temperature on the hardening modulus. The variability is greater in *Figure 10* as compared to *Figure 9*, because the variabilities of both the elastic modulus and tangent modulus measurements are compounded by *Equation (9)*. The uncoupled effects of the hardening modulus are further supported by the results in *Table 2*.

Failure Properties

The p-values calculated through ANOVA for the failure properties are displayed in *Table 5*. Green numbers in *Table 5* indicate that the variable (temperature, moisture, or moisture and temperature) has an impact on the parameter with 95 % confidence, while brown numbers indicate that the variable has no impact on the parameter with 95 % confidence. Therefore, a green number in the *Temperature and Moisture* column shows that the effects of moisture and temperature on the material property are coupled.

The maximum stress results are shown in *Figure 11*. The results displayed in *Figure 11* show a clear coupling of the temperature and moisture effects on maximum stress, as is supported by the results in *Table 5*. This coupling must be due to independent softening

properties of both moisture and temperature on paper, because even a four-percent change in moisture, as was determined in *Figure 3* for high temperatures, does not change the coupled behavior. Unlike the results for C_1 and elastic modulus in the previous section, there does not appear to be an alternate model which can describe the effects of moisture and temperature on C_1 in a non-coupled manner.

The strain at break was defined to be the strain value corresponding to the maximum stress value, which disregards the post-failure behavior. The results of the strain at break are displayed in *Figure 12*. The results in *Figure 12* and *Table 5* show non-coupled effects of moisture and temperature on the strain at break, which is unexpected considering the coupling present for the maximum stress in *Figure 11*. The trends appear to be very linear with the exception of a few outliers at a moisture content of eight percent. Assuming that failure of paper is driven by the maximum stress (which is not necessarily true, as failure of paper is typically driven by a complex coupling of bond and fiber properties [25, 26]), these outliers could be attributed to the fact that, at eight percent moisture content, the maximum stress is still relatively large while the elastic modulus has been dramatically reduced.

Integration of *Equation (4)* up to the strain-at-break value and multiplying by the volume of the test section gives the tensile energy absorption (TEA):

$$TEA = AL_o\left(\frac{C_1 \ln\left(\cosh\left(C_2\varepsilon_{break}\right)\right)}{C_2} + \frac{C_3{\varepsilon_{break}}^2}{2}\right) \tag{10}$$

where A is the cross-sectional area, L_o is the initial length of test section (i.e. the initial distance between the clamps), and ε_{break} is the strain at break. The results for TEA are illustrated in *Figure 13* and *Table 5*. Surprisingly, only temperature has an effect on TEA, whereas moisture and coupled moisture-temperature effects have negligible impact. This result could dramatically simplify the prediction of failure at various moisture-temperature conditions.

The plastic strain was approximated by:

$$\varepsilon_p = \varepsilon_{max} - \frac{\sigma_{max}}{E} \tag{11}$$

where ε_p is the approximate plastic strain, ε_{max} is the strain at break, σ_{max} is the maximum stress, and E is the elastic modulus. The approximate plastic strain provides an estimation of the 3-D formability of the material at various moisture-temperature combinations. *Equation (11)* comes from the assumptions that paper is a linearly elastic material and that the total strain is a sum of elastic and plastic strains. This is an approximate method of calculating the plastic strain that is criticized for its use with paper by Land et al. [9]; for the purpose of these tests, however, *Equation (11)* provides at least a rough estimate of the final plastic strain. The actual plastic strain would be somewhat less than the approximate plastic strain, because the elastic modulus is reduced during plastic straining [27]. The results for the approximate maximum plastic strain are shown in *Figure 14* and *Table 5*. *Figure 14* shows an unexpectedly uncoupled effect of moisture and temperature on the approximate maximum plastic strain. More coupling was expected, because *Equation (11)* is dependent on maximum stress and elastic modulus, both of which show coupled temperature and moisture effects. The outliers at eight percent moisture content are still present, as also seen in *Figure 12*. Apart from the outliers at eight percent moisture content, however, the trends are remarkably linear and uncoupled.

Conclusion

A test method was developed to conduct tensile testing at various moisture content and temperature conditions. The effects of the application of temperature on the moisture content were determined to cause an acceptable level of uncertainty which could slightly alter but not ruin the quality of the results.

The effects of moisture and temperature on the entire mechanical response of paper have been illustrated. Coupled effects of moisture and temperature were discovered for maximum stress. Elastic modulus and C_1 were found to have coupled moisture and temperature effects for a linear model, but the use of an exponential model allowed the effects of moisture and temperature to be modeled without coupling. Uncoupled effects of moisture and temperature were found for C_2, C_3, tangent modulus, hardening modulus, strain at break, TEA, and approximate plastic strain. Additionally, TEA was discovered to be only significantly

affected by the temperature, which could simplify any modeling of a failure point. Many of the relationships followed a clear, linear trend which could be utilized in constitutive modeling.

The one-dimensional effects of temperature and moisture on the material properties presented in this paper must first be extrapolated into 3-D space for the development of a complete material model. With such a material model, accurate finite element modeling of advanced 3-D forming processes should be possible.

Appendix A: Moisture Loss Analysis

Utilizing the results presented in *Figure 3*, the amount of moisture loss at each tested environmental condition can be extrapolated as shown in *Table 6*. Each value in *Table 6* represents the maximum amount of moisture loss at that respective test condition. The green-colored numbers represent maximum moisture losses which are known either from *Figure 3* or from the fact that tests without temperature application should retain constant moisture, while the brown-colored numbers were linearly extrapolated from the known results.

The moisture loss during the tests should be greatest for the failure properties, so the effect of the moisture loss on the maximum stress and strain at break results are investigated. The maximum stress results with the adjustments presented in *Table 6* are shown in *Figure 15*. The results displayed in *Figure 15* show that the coupled effects of moisture and temperature are still present. The trends have not changed drastically compared to *Figure 11*.

The results of the strain at break considering the adjustments in *Table 6* are displayed in *Figure 16*. The results in *Figure 16* appear to indicate the same trends as the results without correction for moisture loss in *Figure 12*. While the moisture loss has some impact on the results, the trends and appearance of coupling do not appear to be considerably affected by the loss of moisture.

Determining the actual amount of moisture loss during each test would be difficult and require many assumptions. Therefore, not adjusting for moisture loss is determined to be the least biased method to present the experimental results. The results which are not corrected for moisture loss are assumed to capture the trends and coupling of the effects of moisture and temperature on each parameter.

Appendix B: Measurement Error Analysis

Sources and magnitudes of possible measurement error are displayed in *Table 7*. Utilizing the first five possible measurement errors (displacement, force, width, thickness, and test length) in *Table 7*, estimates of the error induced into the numerical results caused by the test measurement system can be analyzed for each

load case. The results of these analyses are displayed in *Table 8*. The maximum effects of the possible measurement error on each parameter as well as the measurements which dominate the errors are presented in *Table 8*. The errors on the three curve-fitting parameters for the hyperbolic tangent function (C_1, C_2 and C_3) are not presented, because determining the maximum measurement error on those parameters is not trivial. Additionally, the maximum error for those parameters is expected to be approximately the same magnitude as the errors presented in *Table 8*.

The thickness of paper sheets varies considerably, especially in hand sheets like the ones utilized in this study. This thickness variation causes the greatest measurement error throughout the results. The other two factors which dominate the error magnitude are the specimen length and the strain range utilized in calculating the tangent modulus. The specimen length was limited by the temperature application method, while the strain range was limited by the length of the hardening regions (i.e. the region during which both reversible and irreversible straining occurs) for specimens with a small plastic straining region. Reducing these sources of measurement error would be difficult given the requirements of the temperature application method and given the testing condition at high temperature and low moisture content.

The errors in *Table 8* are expected only in worst-case scenarios, so actual error values much less than these are expected. Therefore, the results should not be significantly affected by the possible measurement errors.

Table 8 does not take into consideration the potential moisture loss and the temperature error. The moisture content and temperature changes according to *Table 7* would cause shifts along the horizontal axis for the figures presented in the results section of this paper, while the errors in *Table 8* would cause shifts along the vertical axis for those figures.

Acknowledgements The authors would like to acknowledge and thank BiMaC Innovation and its industrial partners for their financial support of this research. Additionally, the authors would like to thank Per Larsson and the Department of Fibre and Polymer Technology at KTH Royal Institute of Technology for their assistance with preparing the handsheets and Magnus Gimåker and Innventia for their assistance with pulp beating.

References

1. Östlund, M., Borodulina, S., Östlund, S. (2011). Influence of paperboard structure and processing conditions on forming of complex paperboard structures. Packag Technol Sci 24, 331–341
2. Hauptmann, M., Majschak, J.P. (2011). New quality level of packaging components from paperboard through technology improvement in 3D forming. Packag Technol Sci 24, 419–432
3. Vishtal, A., Retulainen, E. (2012). Deep-drawing of paper and paperboard: the role of material properties. BioResources 7(3), 4424–4450

4. Groche, P., Huttel, D., Post, P.P., Schabel, S. (2012). Experimental and numerical investigation of the hydroforming behavior of paperboard. Prod Engineer 6, 229–236
5. Huang, H., Nygårds, M. (2010). A simplified material model for finite element analysis of paperboard creasing. Nord Pulp Pap Res J 25(4), 505–512
6. Xia, Q.S., Boyce, M.C., Parks, D.M. (2002). A constitutive model for the anisotropic elastic-plastic deformation of paper and paperboard. Int J Solids Struct 39, 4053–4071
7. Mäkelä, P., Östlund, S. (2003). Orthotropic elastic-plastic material model for paper materials. Int J Solids Struct 40, 5599–5620
8. Yokoyama, T., Nakai, K. (2006). Tensile stress-strain properties and fracture resistance of paper and paperboard. SEM Annual Conference and Exposition on Experimental and Applied Mechanics, SEM (2006)
9. Land, C., Wahlström, T., Stolpe, L., Beghello, L. (2010). Plastic strain of moisture streaks at different moisture contents. Nord Pulp Pap Res J 25(4), 481–487
10. Yeh, K., Considine, J., Suhling, J. (1991). The influence of moisture content on the non-linear constitutive behavior of cullulosic materials. pp. 695–711. International Paper Physics Conference (1991)
11. Haslach, Jr., H.W. (2000). The moisture and rate-dependent mechanical properties of paper: A review. Mech Time-Depend Mat 4, 169–210
12. Haslach, H. (2009). Time-dependent mechanisms in fracture of paper. Mech Time-Depend Mat 13, 11–35
13. Gunderson, D., Considine, J., Scott, C. (1988). The compressive load-strain curve of paperboard: rate of load and humidity effects. J Pulp Paper Sci 14, 713–726
14. Nissan, A.H. (1976). H-bond dissociation in hydrogen bond dominated solids. Macromolecules 9(5), 840–850
15. Erkkilä, A.L., Leppänen, T., Hämäläinen, J. (2013). Empirical plasticity models applied for paper sheets having different anisotropy and dry solids content levels. Int J Solids Struct 50, 2151–2179
16. Benson, R.E. (1971). Effects of relative humidity and temperature on tensile stress-strain properties of kraft linerboard. Tappi J 54(5), 699–703
17. Ek, M., Gellerstedt, G., Henriksson, G. (2009). Paper Products Physics and Technology, Pulp and Paper Chemistry and Technology, vol. 4, chapter 4, pp. 109–143. De Gruyter, Berlin
18. Berthold, J., Desbrières, J., Rinaudo, M., Salmén, L. (1994). Types of adsorbed water in relation to the ionic groups and their counter-ions for some cellulose derivatives. Polymer 35(26), 5729–5736
19. Luukkonen, P., Maloney, T., Rantanen, J., Paulapuro, H., Yliruusi, J. (2001). Mircrocrystalline cellulose-water interaction – a novel approach using thermoporosimetry. Pharmaceut Res 18(11), 1562–1569
20. Salmén, N.L., Back, E.L. (1977). Simple stress-strain measurements on dry papers from -25°c to 250°c. Sven Papperstidn 80(6), 178–183

21. Salmén, N.L., Back, E.L. (1978). Effect of temperature on stress-strain properties of dry papers. Sven Papperstidn 81(10), 341–346
22. Salmén, N.L., Back, E.L. (1980). Moisture-dependent thermal softening of paper evaluated by its elastic modulus. Tappi J 63(6), 117–120
23. Hagman, A., Nygårds, M. (2012). Investigation of sample-size effects on in-plane tensile testing of paperboard. Nord Pulp Pap Res J 27(2), 295–304
24. Gunderson, D. (1991). Method for measuring mechanosorptive properties. J Pulp Pap Sci 17(2), J53–J59
25. Borodulina, S., Kulachenko, A., Galland, S., Nygårds, M. (2012). Stress-strain curve of paper revisited. Nord Pulp Pap Res J 27(2), 318–328
26. Isaksson, P., Gradin, P., Kulachenko, A. (2006). The onset and progression of damage in isotropic paper sheets. Int J Solids Struct 43, 713–726
27. Coffin, D.W. (2012). Use of the efficiency factor to account for previous straining on the tensile behavior of paper. Nord Pulp Pap Res J 27(2), 305–312

Tables

Table 1 Tested moisture-temperature combinations

mc \ T	23 ^{o}C	60 ^{o}C	114 ^{o}C	148 ^{o}C	168 ^{o}C
6.9 %	X	X	X	X	X
8 %	X		X		X
9 %	X		X		X
10.6 %	X		X		X
13.9 %	X		X		X

Table 2 p-value results for the constitutive properties from ANOVA

Parameter	**Temperature**	**Moisture**	**Temperature and Moisture**
C_1	0.0000	0.0000	0.0024
C_2	0.0000	0.0000	0.2683
C_3	0.0000	0.0053	0.8845
Elastic Modulus	0.0000	0.0000	0.0045
Tangent Modulus	0.0000	0.0000	0.3733
Hardening Modulus	0.0000	0.0000	0.5888

Table 3 Non-linear regression results for C_1

Constant	p-value
β_1	0.0000
β_2	0.0000
β_3	0.0001
β_4	0.1264

Table 4 Non-linear regression results for the elastic modulus

Constant	p-value
β_1	0.0000
β_2	0.0000
β_3	0.0002
β_4	0.0508

Table 5 p-value results for the failure properties from ANOVA

Parameter	Temperature	Moisture	Temperature and Moisture
Maximum Stress	0.0000	0.0000	0.0000
Strain at Break	0.0000	0.0000	0.8734
Tensile Energy Absorption (TEA)	0.0000	0.1900	0.4645
Approximate Max Plastic Strain	0.0000	0.0000	0.3853

Table 6 Maximum changes of moisture content at specimen failure

mc \ T	23 ^{o}C	60 ^{o}C	114 ^{o}C	148 ^{o}C	168 ^{o}C
6.9 %	0 %	0.2 %	0.5 %	0.7 %	0.8 %
8 %	0 %		0.8 %		1.3 %
9 %	0 %		1.1 %		1.7 %
10.6 %	0 %		1.5 %		2.4 %
13.9 %	0 %		1.9 %		3.0 %

Table 7 Sources and magnitudes of possible measurement error

Type	Maximum Error
Displacement Measurement	± 0.01 mm
Force Measurement	± 0.25 %
Specimen Width	± 0.2 mm
Specimen Thickness	± 10 μm (one standard deviation)
Specimen Test Length	± 1 mm
Moisture Content Loss	-4 % mc
Applied Temperature	± 5 ^{o}C

Table 8 Maximum possible measurement error on the parameters

Parameter	Max Error	Dominating Error
Maximum Stress	± 5 %	Thickness
Strain at Break	± 3 %	Specimen Length
Plastic Strain	± 7 %	Thickness & Specimen Length
Elastic Modulus	± 6 %	Thickness
Tangent Modulus	± 11 %	Strain Range Utilized
Hardening Modulus	± 13 %	Strain Range Utilized

Figures

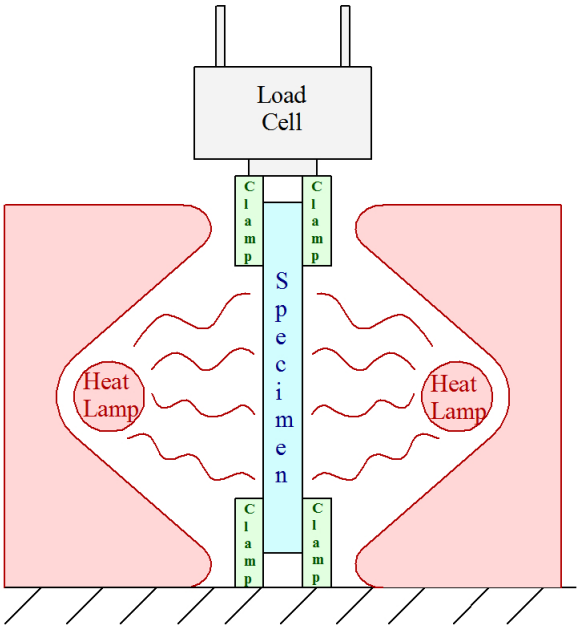

Fig. 1 Illustration of the tensile test setup

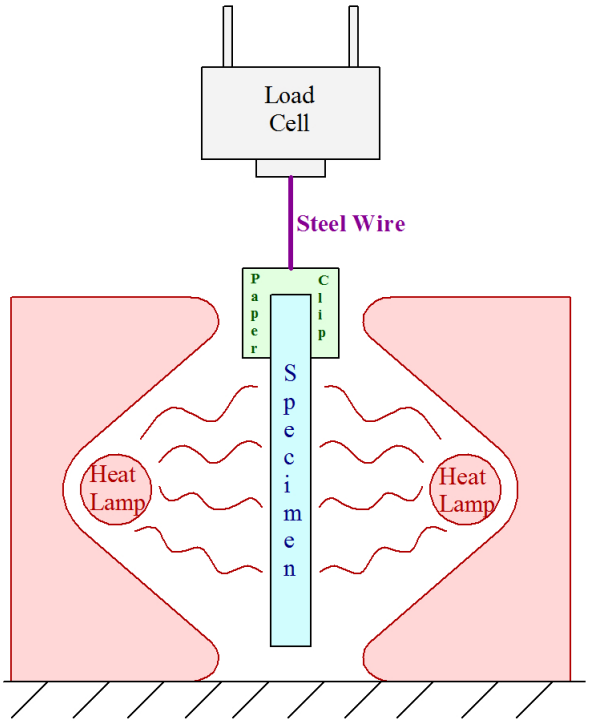

Fig. 2 Test setup to analyze the moisture loss during heat application

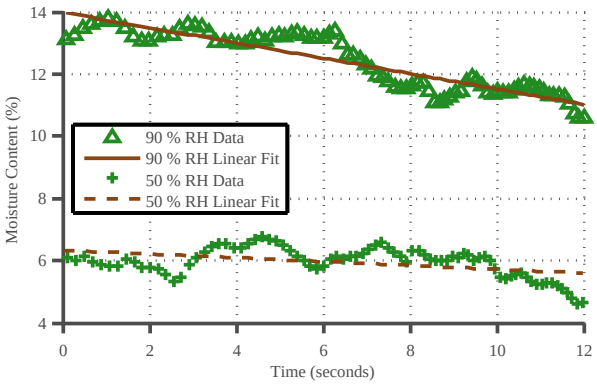

Fig. 3 Moisture loss at high humidity and high temperature

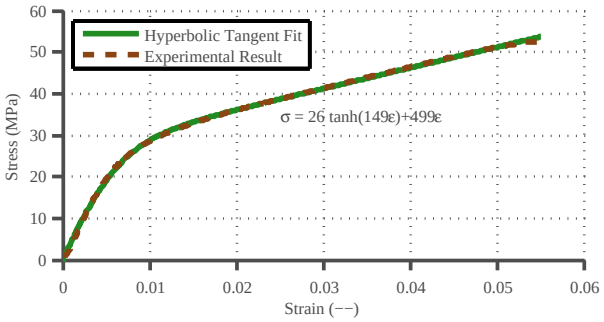

Fig. 4 An example of the hyperbolic tangent function

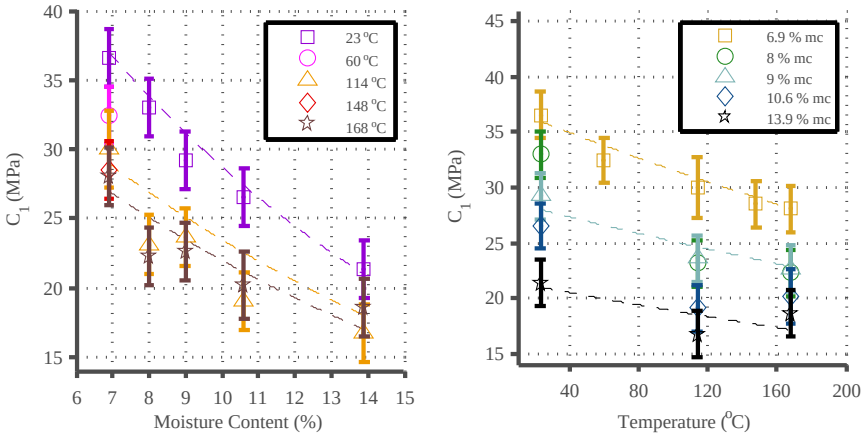

Fig. 5 Dependency of C_1 on moisture and temperature

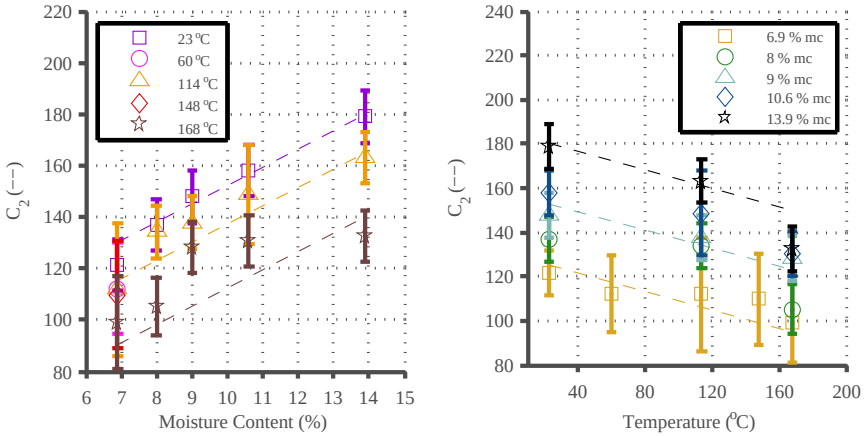

Fig. 6 Dependency of C_2 on moisture and temperature

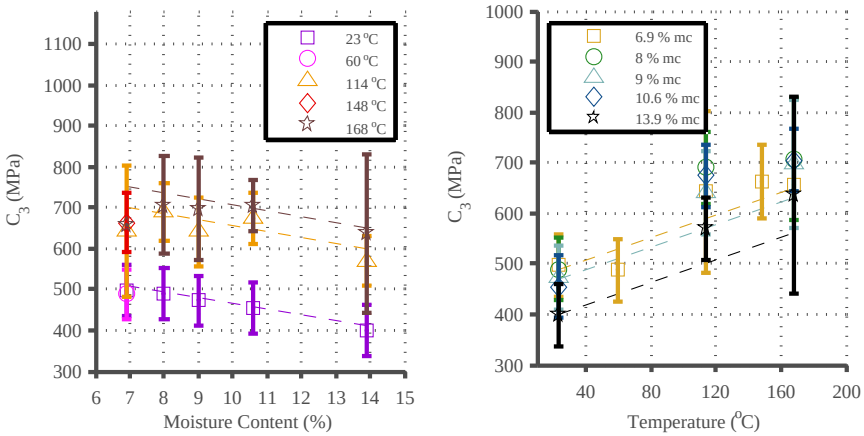

Fig. 7 Dependency of C_3 on moisture and temperature

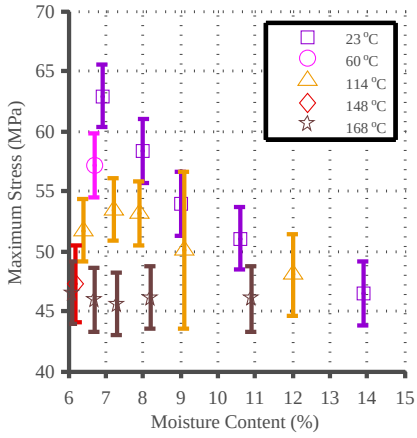

Fig. 15 Dependency of maximum stress on moisture and temperature including moisture loss

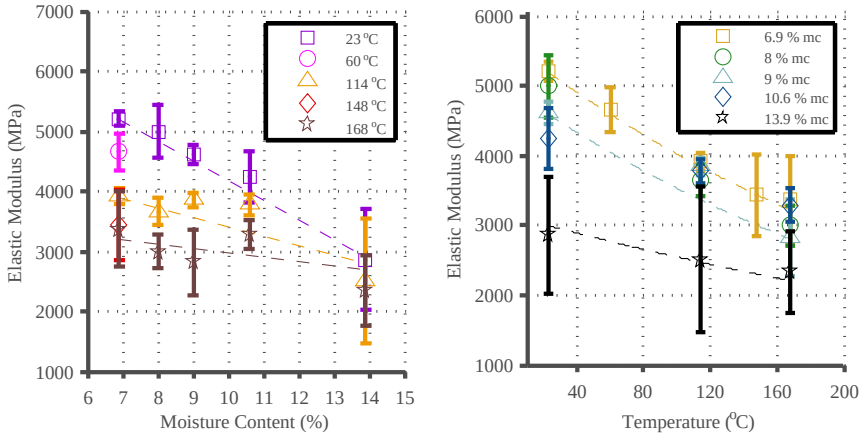

Fig. 8 Dependency of elastic modulus on moisture and temperature

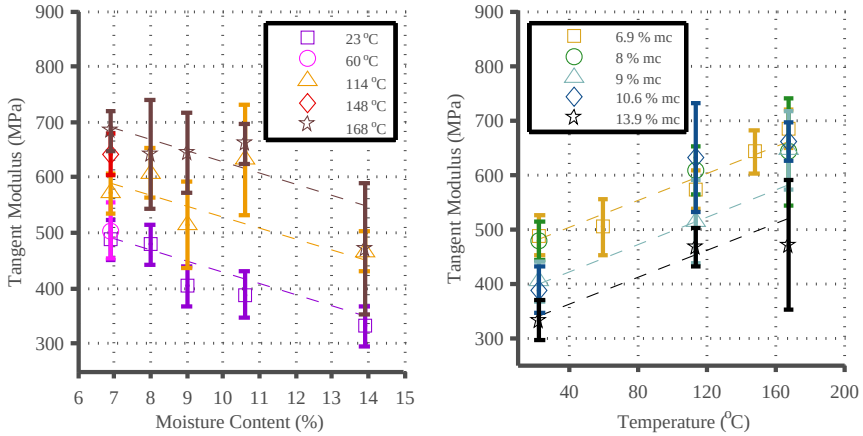

Fig. 9 Dependency of tangent modulus on moisture and temperature

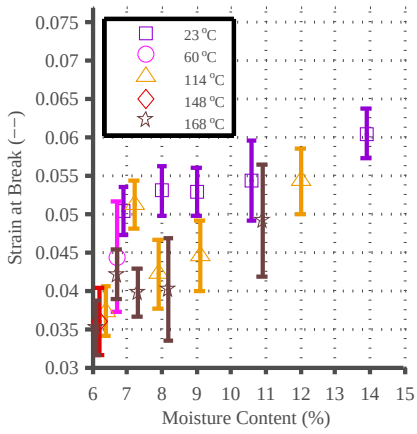

Fig. 16 Dependency of strain at break on moisture and temperature including moisture loss

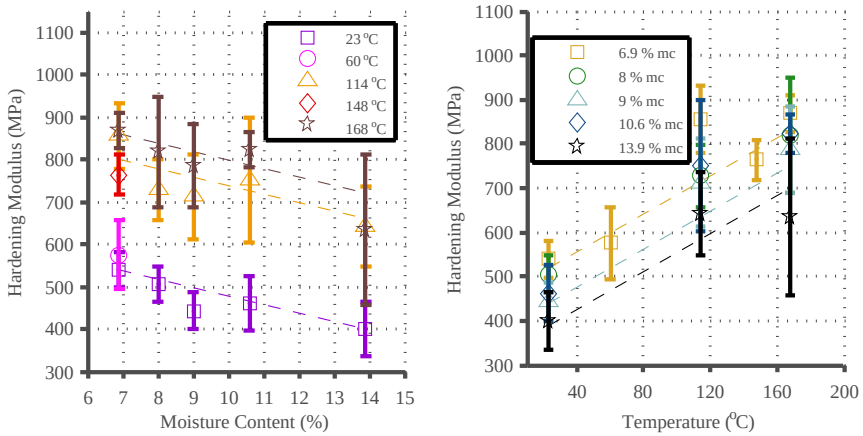

Fig. 10 Dependency of hardening modulus on moisture and temperature

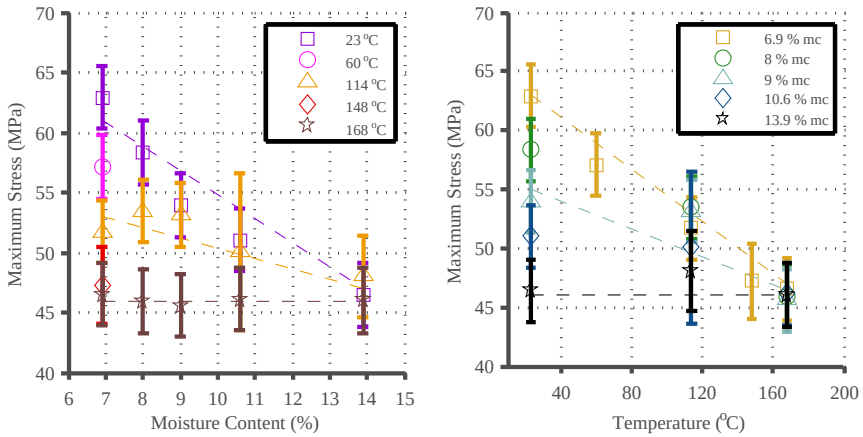

Fig. 11 Dependency of maximum stress on moisture and temperature

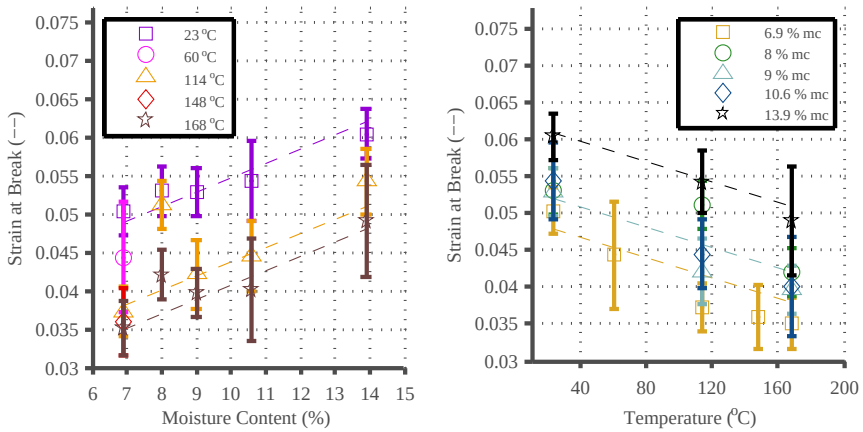

Fig. 12 Dependency of strain at break on moisture and temperature

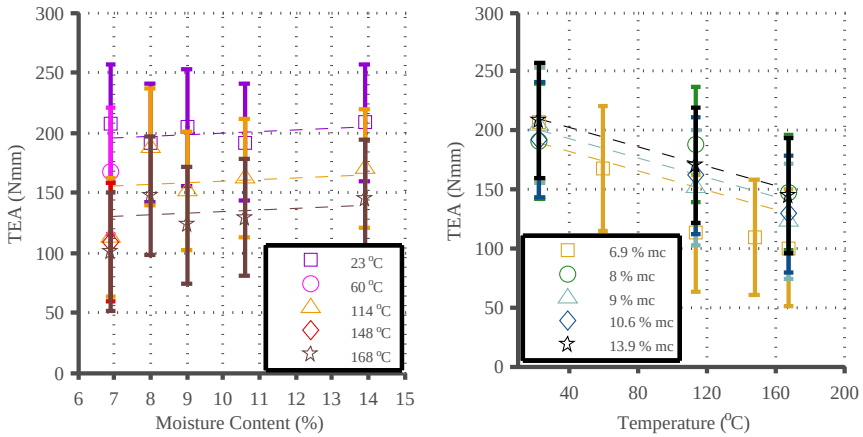

Fig. 13 Dependency of TEA on moisture and temperature

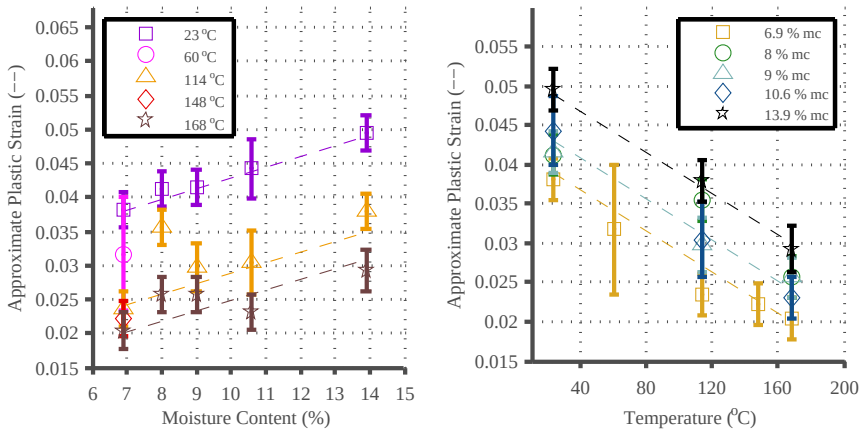

Fig. 14 Dependency of approximate maximum plastic strain on moisture and temperature